# Finite-Element Solution of Unbounded Field Problems

BRUCE H. MCDONALD AND ALVIN WEXLER

*Abstract*—An unbounded region is divided into local picture-frame regions where a partial differential-equation solution is obtained, with the remaining unbounded region represented by an integral equation. (The method permits the use of free-space Green's functions, and thus special problem-dependent Green's functions need not be found.) The integral equation is formulated as a constraint upon the local picture-frame solutions, whence these local solutions are solved directly by a variational method, using finite elements, in a manner such that the problem of the Green's-function singularity is side-stepped. The technique is applicable where sources and media inhomogeneities and anisotropies are local, and can all be placed within one or several picture frames. It is in these cases that the integral-equation approach is at a particular disadvantage, and the use of a partial differential-equation technique is advisable if not necessary. Examples presented include the static and harmonic fields of a parallel-plate capacitor, a microstrip line on a dielectric substratum, and a radiating antenna with dielectric obstacles.

## I. Introduction

FIELD PROBLEMS, where the region of interest is bounded, are customarily solved by formulating a partial differential equation and using knowledge of the boundary conditions to obtain the solution. When the region of interest is unbounded it is customary to use an integral-equation method to obtain a local charge distribution, and from this the fields as required. Integral equations often possess singular kernels that can produce "algorithmic nightmares" [1], and such methods depend upon the existence of an "action-at-a-distance" Green's function that may be very difficult to find, especially when inhomogeneities or anisotropies occur. Moreover, certain algorithmic niceties about a partial differential-equation solution, along with demonstrable capabilities for handling inhomogeneities and anisotropies, invite the analyst to seek ways of solving unbounded field problems using differential techniques.

If sources, media inhomogeneities, and anisotropies are local, a surface may be defined to enclose them. The internal region so defined is bounded, and differential techniques may be used there. In the remaining unbounded region an integral equation may be formulated using only a simple free-space Green's function. The field at the surface may be interpreted two ways: as a boundary condition for the differential-equation formulation of a boundary-value problem; and as an equivalent source distribution for the exterior integral equation. If continuity of field and first derivatives are enforced between these two formulations at the surface, the problem is readily solved.

When iterative procedures are used to solve this problem, the technique belongs to the well-known class of boundary-relaxation methods. This paper presents a method whereby the bounded region is solved directly by a variational technique using finite elements, with the integral equation as a constraint.

## II. General Description of the Method

A two-dimensional, or plane, problem is discussed in detail, although extension to three-dimensional problems can readily be made.

Fig. 1(a) shows a portion of the infinite $x$–$y$ plane in Cartesian coordinates (for definiteness, $z=0$). A bounded region called a picture frame $R_1$ is placed so as to contain all sources, inhomogeneities, and anisotropies. The boundary of the picture frame is designated $B_1$, and the unbounded exterior region is $R_E$. The picture frame represents a boundary-value problem with boundary conditions as yet unspecified. It is solved by the finite-element method.

We now introduce a closed contour $C_1$, as shown in Fig. 1(b). The region of the plane outside $C_1$ is called $R_c$, and it is stipulated that the region of overlap between $R_c$ and $R_1$ be source free, homogeneous, and isotropic. This is not really a restriction, since the picture frame and contour can be placed as desired.

In the exterior region $R_c$ an integral equation is used to relate the field at any point in $R_c$ to the field (or a function of the field that can be considered as an equivalent charge distribution) on the contour $C_1$. In particular, we evaluate the integral equation at points on $B_1$, the picture-frame boundary. This produces a set of constraints upon the picture-frame field that forces it to assume, at the boundary $B_1$, the correct value for the unbounded problem. The overlap region precludes evaluation of the integral equation at a source point, thus side-stepping problems with Green's-function singularities.

Extension to several picture frames is straightforward —a contour $C$ may be defined consisting of a closed contour $C_1$ in each frame with cuts defined between these $C_1$, which disappear in integration and which link the picture frames together. See Fig. 1(c).

The method is applicable to problems having unbounded regions provided that:

1) sources, inhomogeneities, and anisotropies are local, so that they may be completely enclosed within picture frames;

Manuscript received May 30, 1972; revised August 21, 1972. This work was supported by the National Research Council of Canada. This paper was presented at the 1972 IEEE International Microwave Symposium, Chicago, Ill., May 22–24, 1972.

The authors are with the Department of Electrical Engineering, University of Manitoba, Winnipeg, Man., Canada.

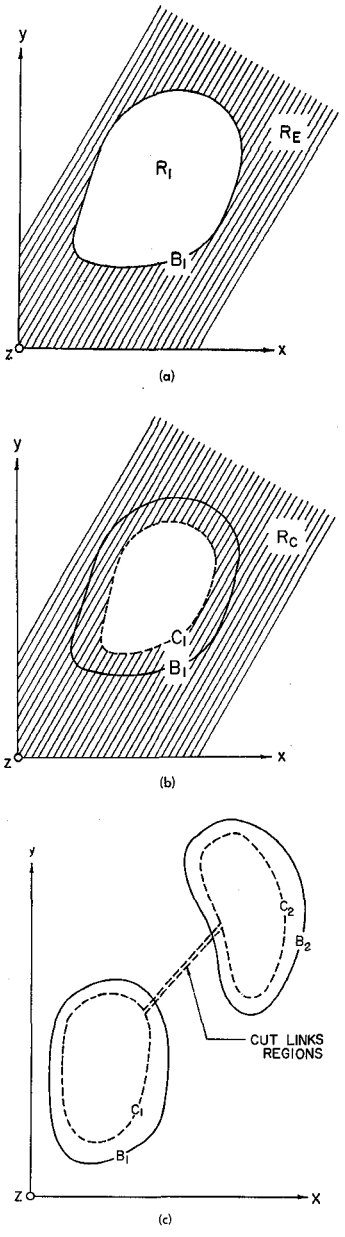


Fig. 1. The infinite plane, the picture frame, and associate contours. (a) The picture frame $R_1$, its boundary $B_1$, and the external region $R_E$. (b) The contour $C_1$ and the region external to it $R_C$. (c) The linking of two picture frames.

2) a free-space Green's function exists;
3) local picture-frame solutions are constructed so that field values at the boundary can be linearly expressed in terms of field values on the contour $C_1$.

Physically, it is possible to interpret the exterior integral-equation formulation as the replacement of the picture-frame solution by an equivalent-source or charge distribution along the contour $C_1$. Alternatively, the picture-frame solution involves the replacement of the free-space problem by an equivalent-boundary condition on $B_1$.

Static and harmonic electromagnetic-field problems are easily solved, and the finite-element method readily admits the linear constraint equations.

## III. Previous Work

Several related schemes have recently been reported, which, in the main:

1) have used finite-difference techniques for the picture-frame solutions;
2) have been used for only one picture frame, with no indication otherwise;
3) have been restricted to Laplace's equation;
4) have had to cope with singularities of Green's functions.

Silvester and Cermak [2], [3] in effect chose $C_1$ very close to $B_1$ within one grid point in their finite-difference representation. This choice allows a direct linking of potentials on $C_1$ and $B_1$ with finite differences, but introduces problems with Green's-function singularities. The scheme does not preclude choosing $C_1$ further away from $B_1$, although such a choice would require additional equations to relate potentials, and could possibly affect convergence of the iterative process.

More recently Silvester and Hsieh [4] have applied finite elements, using a functional which effectively minimizes energy in all space, including $R_E$. This approach appears to be limited to the Laplace operator (where total energy is finite), and the problem of singularity of the Green's function remains.

Sandy and Sage [5] in effect choose $C_1$ to lie along the surface of a conductor in the picture frame (a TEM microstrip problem). Problems with Green's-function singularities are avoided, since potentials are not evaluated at source points. They use an iterative procedure to obtain their solution, beginning with an estimate of potential on $B_1$, evaluating the field by SOR with finite differences to determine sources on $C_1$, and then computing a potential for $B_1$ from the integral equation. This potential is used to make a better estimate, and the procedure recycles. They point out that convergence is not guaranteed, and, in fact, use underrelaxation to improve their estimate for potential on $B_1$. Computation time is undoubtedly high, and media inhomogeneities must be very carefully provided for. Their technique permits sources outside the picture frame when these can be added as a lumped contribution.

Greenspan and Werner [6] discuss a finite-difference approach for the Helmholtz operator, and show that solutions do exist, are unique, and can be numerically obtained. The contour $C_1$ is taken coincident with $B_1$, thus producing singularity problems.

## IV. The Finite-Element Method

The finite-element method, used to produce a field solution for a bounded region, such as $R_1$ in Fig. 1, is described in detail by Silvester [16], and Richards and Wexler [7], with extension to provide for anisotropic, continuously inhomogeneous regions given by Wexler [8]. The book by Zienkiewicz [18] is also a good reference.

Using the example of Poisson's equation in a continu-

ous inhomogeneous region, we have

$$-\nabla\cdot(\epsilon\nabla\phi) = f \qquad \text{within } R_1. \tag{1}$$

The quadratic functional is discussed fully in [14, pp. 291–318], and using the forms given in [17, eqs. (96) and (112)], we have, in general

$$F = \int_{R_1} \epsilon\nabla\phi^*\cdot\nabla\phi\, dxdy - \int_{R_1}\phi f^*\, dxdy - \int_{R_1}\phi^* f\, dxdy \tag{2a}$$

$$F = \int_{R_1}\epsilon\left|\nabla\phi\right|^2 dxdy - 2\,\mathrm{Re}\left\{\int_{R_1}\phi f\, dxdy\right\} \tag{2b}$$

where clearly $\nabla\phi^*\cdot\nabla\phi = |\nabla\phi|^2$. The superscript $*$ denotes the complex conjugate. For positive $\epsilon$, $F$ possesses the desirable characteristic of positive definiteness.

The field within $R_1$ is represented by a combination of appropriate polynomial interpolatory functions $\alpha_j$, defined on an element basis, and node potentials $\phi_j$, which are field values at $n$ specific points in $R_1$

$$\phi = \sum_{j=1}^{n}\alpha_j\phi_j \tag{3a}$$

where by definition $\alpha_j$ takes on the values

$$\alpha_j = \begin{cases} 1, & \text{at node } j \\ 0, & \text{at other nodes.} \end{cases} \tag{3b}$$

The subscript $j$ refers to node positions, some internal (subscripted $I$) and some on the boundary (subscripted $B$). Then, in vector notation, (3a) may be written

$$\phi = \boldsymbol{\alpha}_B{}^T\phi_B + \boldsymbol{\alpha}_I{}^T\phi_I = \phi_B{}^T\boldsymbol{\alpha}_B + \phi_I{}^T\boldsymbol{\alpha}_I. \tag{4}$$

We may define four matrices, $A_{II}$, $A_{IB}$, $A_{BI}$, and $A_{BB}$, for example

$$A_{BI} = \int_{R_1}\epsilon\nabla\boldsymbol{\alpha}_B\nabla\boldsymbol{\alpha}_I{}^T\, dxdy \tag{5}$$

and vectors $\boldsymbol{b}_I$ and $\boldsymbol{b}_B$, for example

$$\boldsymbol{b}_I = \int_{R_1}\boldsymbol{\alpha}_I f\, dxdy. \tag{6}$$

The integral-equation constraint produces a linear relationship between $\phi_B$ and $\phi_I$, which is written, as shown in Section V, (17)

$$\phi_B = M\phi_I. \tag{7}$$

Now we make use of (4)–(7) to rewrite (2)

$$F = \phi_I{}^T\{A_{II} + A_{IB}M + M^TA_{BI} + M^TA_{BB}M\}\phi_I - 2\phi_I{}^T\{\boldsymbol{b}_I + M^T\boldsymbol{b}_B\}. \tag{8}$$

Positive definiteness of the functional is not altered by the substitutions. At the solution point, $F$ is a minimum and its derivative with respect to the vector $\phi_I$ is a zero vector. Performing this differentiation, and equating this derivative to a zero vector, we obtain the positive-definite system

$$[A_{II} + A_{IB}M + M^TA_{BI} + M^TA_{BB}M]\phi_I = \boldsymbol{b}_I + M^T\boldsymbol{b}_B. \tag{9}$$

The matrices produced by this finite-element formulation are smaller in size but more dense than finite-difference matrices. The problems presented here consist of about 60 unknowns. Although these matrices may be block sparse with an appropriate node ordering system, permitting large problems to be solved by block-iterative techniques, they are treated here as being dense.

Types of errors occurring in the finite-element method are discussed in [7], along with some indication of computer-time requirements.

For the case of several picture frames, the representation is extended to include all nodes in all picture frames, and the derivation proceeds identically.

The finite-element method provides good solutions when the field is naturally polynomic or close to polynomic. Derivative singularities, such as those occurring at edges of conductors, are not well approximated. Extensions of the finite-element method to provide for such singularities are presented by Décreton and Wexler [9]; much improved accuracy is obtained.

The Helmholtz operator alters the functional slightly, and positive definiteness is guaranteed only for frequencies below the lowest eigenfrequency of any picture-frame region. These regions should therefore be kept sufficiently small to ensure that this is so. This will be discussed in a subsequent publication.

## V. The Integral-Equation Constraint

In the region outside $C_1$ in Fig. 1(b), which we have called $R_c$, Laplace's equation holds

$$\nabla^2\phi(x, y) = 0. \tag{10}$$

Also, the Green's relation

$$-\nabla^2 G(x, y\,|\,x_0, y_0) = \delta(x - x_0, y - y_0) \tag{11}$$

is applicable, and since $R_c$ is assumed to be source free, homogeneous, and isotropic, the free-space Green's function may be used

$$G(x, y\,|\,x_0, y_0) = -\frac{1}{2\pi\epsilon_0}\ln\sqrt{(x - x_0)^2 + (y - y_0)^2}. \tag{12}$$

Multiplying (10) by $G$, (11) by $\phi$, adding the resulting equations, and integrating over $R_c$, we obtain

$$\phi(x, y) = \int_{R_c}\{G(x, y\,|\,\xi, \rho)\nabla^2\phi(\xi, \rho) - \phi(\xi, \rho)\nabla^2 G(x, y\,|\,\xi, \rho)\}\, d\xi d\rho \tag{13}$$

for any point $(x, y)$ in $R_c$. Applying Green's theorem, we obtain:

$$\phi(x, y) = \oint_{C_1}\left(G\frac{\partial\phi}{\partial n} - \phi\frac{\partial G}{\partial n}\right) ds. \tag{14}$$

Note that $C_1$ is only part of a larger closed-contour $C$, the outer parts of which are cuts which disappear in integration, and a part at infinity whose contribution to the integration vanishes. See Stakgold [10, pp. 142–143].

Field quantities on $C_1$ in (14) may be represented by the node functions and potentials given by (4)

$$\phi = \left\{ \oint_{C_1} \left( G \frac{\partial \alpha_I^T}{\partial n} - \alpha_I^T \frac{\partial G}{\partial n} \right) ds \right\} \phi_I + \left\{ \oint_{C_1} \left( G \frac{\partial \alpha_B^T}{\partial n} - \alpha_B^T \frac{\partial G}{\partial n} \right) ds \right\} \phi_B. \quad (15)$$

Once all node potentials are established, (15) is used to determine the field at any point in space outside the picture frame.

To produce the constraint equation, (15) is evaluated at all node points on the boundary $B_1$. Thus

$$\phi_B = P_I \phi_I + P_B \phi_B \quad (16)$$

where rows of the matrices $P_I$ and $P_B$ are determined from (15) and evaluated for each of the boundary node points.

An adjustment of (16) puts it into the form of (7)

$$\phi_B = (I - P_B)^{-1} P_I \phi_I = M \phi_I. \quad (17)$$

Again there is no restriction to just one picture frame. If more than one picture frame is employed, each has its own boundary nodes and contour $C_1$. The derivation proceeds similarly for the Helmholtz Green's function, excepting that complex arithmetic must be used.

Contour integration along $C_1$ is performed numerically using the trapezoidal rule at present; three-figure accuracy is easily obtained. The computer time required for these integrations has been found not to exceed 30 percent of that required to build the finite-element matrices.

## VI. Examples

Several examples are presented using the method described. The square parallel-plate capacitor shows the accuracy of the scheme for an electrostatic problem, while other examples show placement of dielectric material, harmonic-field problems, and the use of several picture frames in one problem.

### A. The Square Parallel-Plate Capacitor

A cross section of the geometry is shown in Fig. 2(a), representing two infinitely long, thin, conducting plates of width equal to their separation. A single picture-frame boundary and contour are labelled $B_1$ and $C_1$, respectively. Considering the symmetries involved, the solution can be obtained in the positive quadrant, and, accordingly, finite elements are placed there. This reduced picture frame is bounded by one-quarter of $B_1$, where the integral constraint is applied, and by parts of the $x$ and $y$ axes, where homogeneous Dirichlet and

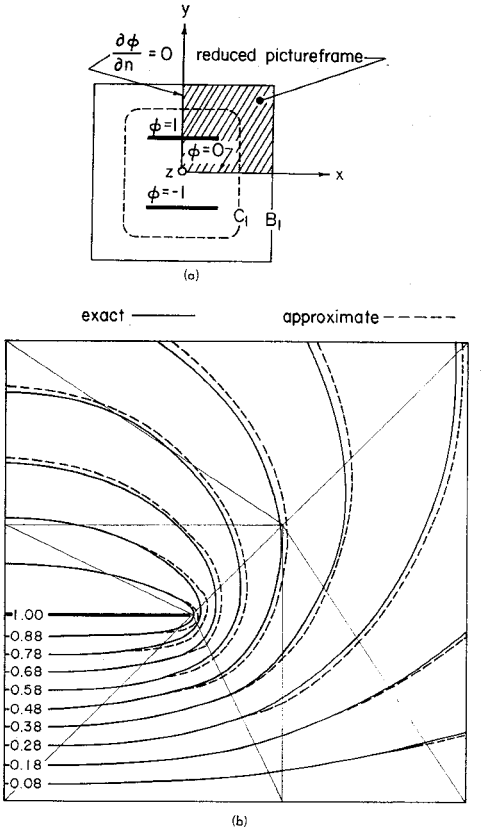


Fig. 2. The parallel-plate capacitor. (a) Cross section showing the picture frame. (b) Electrostatic equipotentials in the reduced picture frame.

Neumann boundary conditions are imposed, respectively, to provide for the symmetries. Integration along the contour $C_1$ is facilitated by choosing it symmetrically, in order that appropriately signed images of the field values in the positive quadrant may be used in the other three.

The edge of the capacitor plate within the reduced picture frame causes a derivative singularity. Triangular finite elements are judiciously placed in order to minimize this effect, as shown in Fig. 2(b). A Dirichlet boundary condition of 1 V is specified on the plate, and the electrostatic solution is obtained using fourth-order polynomials of the form $x^m y^n$ [7], which results in 65 interior node potentials, the unknowns in (9).

Capacitance is computed from the electrostatic energy of the field obtained by an integration of $(\nabla\phi)^2$ over the picture frame plus an integration of $\phi\, \partial\phi/\partial n$ along $B_1$, the picture frame boundary [4]. With free-space permittivity assumed throughout, the capacitance is computed to be 18.9 pF/m. An equipotential plot of the solution within the picture frame is shown as the dashed lines in Fig. 2(b).

Several methods are available to determine the exact capacitance [11]–[13], which is given as 18.7 pF/m, indicating our value to be high by about 1 percent. The derivative singularity no doubt contributes to this error, while the nature of the convergence of the finite-element method predicts an energy (and hence capacitance) higher than the correct value. As Mikhlin [14, ch. II]

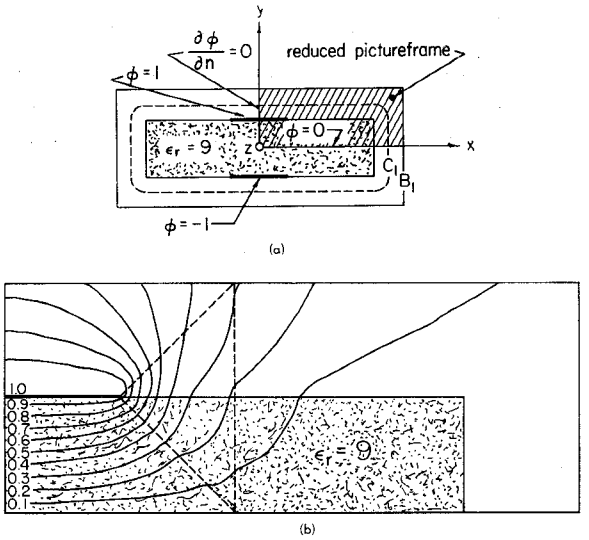


Fig. 3. Parallel plates with dielectric slab $\epsilon_r=9$. (a) Cross section showing the picture frame. (b) Electrostatic equipotentials in the reduced picture frame.

points out, the positive-definite functional (2) produces a minimizing sequence in the energy sense, with exact convergence occurring in the limit only with an energy-complete function set. Therefore, our computed capacitance is an upper bound, but is not a least upper bound since our set of polynomials is not energy complete.

An "exact" equipotential plot, shown as solid lines in Fig. 2(b), is obtained by solving, with care, the relevant integral equation [1], and is reliable to three significant figures. Discrepancies near the edge of the plate are observed, while the equipotential plot tends to exaggerate errors in the relatively flat field near the picture-frame boundary. The constrained finite-element solution of the field within the picture frame is clearly quite good, and does represent a snapshot of the entire field.

### *B. Square Capacitor with a Dielectric Slab*

Fig. 3(a) shows, in cross section, an infinitely long slab of dielectric ($\epsilon_r=9$), filling the space between the plates and extending outward from the edges a small distance. This configuration resembles some microstrip problems discussed in the literature [11], [12], although normally the slab is taken as being infinitely wide as well as long. Following identically the steps of the previous example, the reduced picture frame is solved producing the equipotential plot shown in Fig. 3(b). Electrostatic energies are used ([4] and [12]) to compute an effective dielectric constant of 6.38. Since most of the energy in the dielectric is concentrated near the plates, an infinitely wide dielectric slab should produce a dielectric constant just slightly higher; Bryant and Weiss [12] published 6.47, which is about 1 percent higher than our value.

The effect of the derivative singularity is clearly observed [Fig. 3(b)] in the wobble of the equipotentials in the two triangular elements (indicated by dashed lines) abutting the edge of the plate. (The other elements are not indicated.)

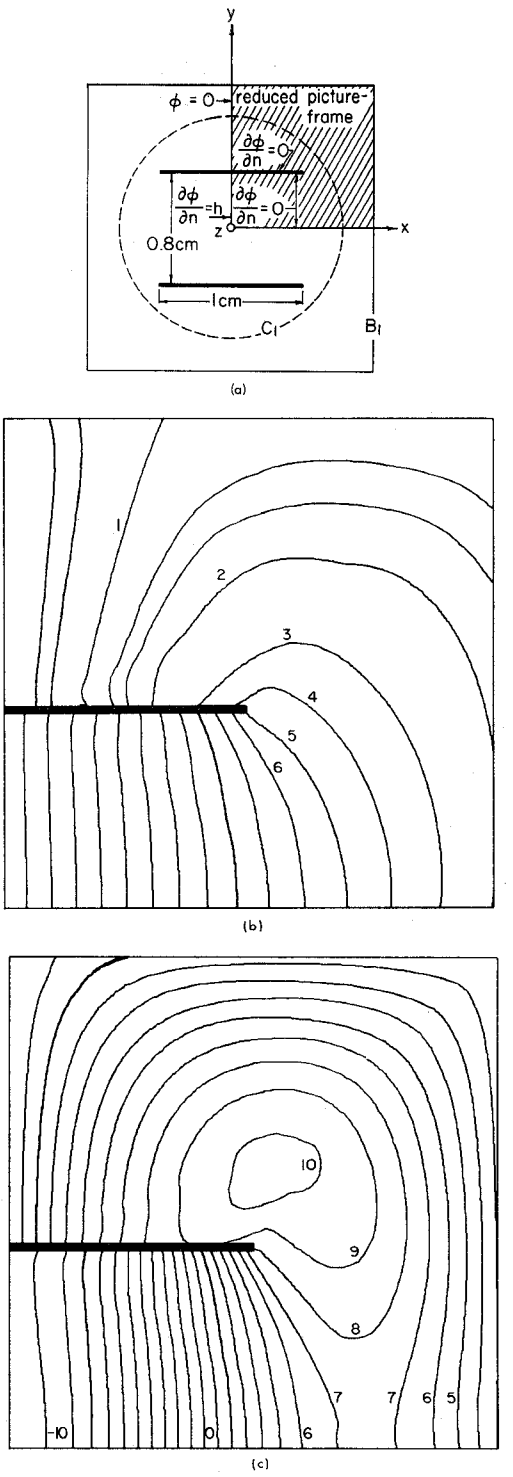


Fig. 4. Parallel plates, using electric vector potential, with static and harmonic solutions. (a) Cross section showing the picture frame. (b) Static solution, with contours proportional to $H_z$. (c) Harmonic solution, with contours proportional to $H_z$, at 19 GHz at phase zero, in the reduced picture frame.

### *C. Parallel Plates; the Harmonic Problem*

For this example, the $z$-directed electric-vector potential is used. Equipotentials, then, are proportional to contours of constant $H_z$ and prescribe the direction of the electric field (see [15, pp. 129–131]).

Fig. 4(a) shows a familiar geometry—infinitely long parallel plates with specified dimensions. Symmetry

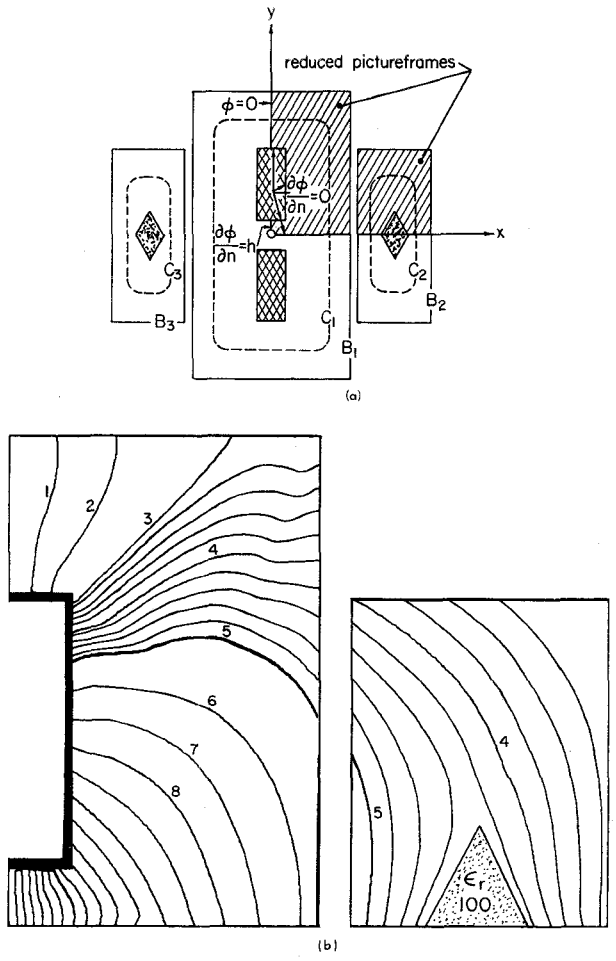


Fig. 5. Antenna-type problem with dielectric obstacles using 3 picture frames. (a) Cross section showing the picture frames. (b) Harmonic solution, contours proportional to $H_z$, at 5 GHz, at phase zero, in the reduced picture frames.

conditions are used to reduce the picture frame, with appropriate axis boundary conditions. A line dipole source is connected across the plates at the origin, producing the inhomogeneous Neumann boundary condition shown. Free-space media constants are assumed throughout, and a homogeneous Neumann boundary condition is specified on the plate.

Fig. 4(b) shows the static solution. Comparison with Fig. 2(b) shows the effect of the change in potential function, the contours of one being normal to the contours of the other.

Operating the dipole harmonically presents us with the Helmholtz operator. The Green's function is a Hankel function—see [10, p. 266–268] and [15, pp. 198–204] for outward travelling waves, resulting in a complex-valued field. A frequency of 19 GHz produces a marginally positive-definite system, and Fig. 4(c) shows equipotentials of the real part of the field at phase zero. Harrington [15, p. 277] in discussing free-space modes in spherical coordinates, presents the $TM_{01}$ mode, which shows a marked similarity to the contours of Fig. 4(c).

### *D. A Radiating Antenna with Dielectric Obstacles*

Fig. 5(a) shows a cross section of two conducting slabs and two dielectric bars, all infinite in length and parallel. The conducting slabs, about the $x=0$ plane, represent an antenna with a thick-line dipole source connected across the gap between them. The two dielectric bars ($\epsilon_r=100$) represent obstacles, and are placed symmetrically on the $x$ axis. Three picture frames and contours are placed as shown. The symmetry of the problem again permits solution in one positive quadrant, resulting in two reduced picture frames to consider. We proceed to a harmonic solution, using the $z$-directed electric-vector potential, and show equipotentials of $H_z$ [Fig. 5(b)] for the source at 5 GHz at phase zero.

A rather small number of node poetntials was specified with large triangular elements, resulting in some field errors observed in part of the larger picture frame $R_1$. (Finite-difference users might note that 60 nodes represent a very coarse grid. With finite elements much more field information is usually provided by each node potential.) Nevertheless, the field is continuous from one picture frame to the other, as evidenced by the contour numbered 5. Also behavior of the field near the dielectric bar is clearly correct.

Theoretically, the boundaries of the picture frames should be transparent to the final solution. In practice errors do occur, but the error at a picture-frame boundary is no worse than the error at any element interface.

## VII. Conclusions

The use of free-space integral equations to constrain the local finite-element solution in picture frames appears to be entirely satisfactory for the solution of static and time-harmonic problems in unbounded regions. Time is spent solving problems in local regions of interest; none is wasted elsewhere. However, the field at intermediate locations can be computed at small marginal cost. Field values in all space are available from the picture-frame solutions. The finite-element software at hand permits analysis with sources, inhomogeneities, and anisotropies, when these can all be placed within picture frames, and its power will be greatly enhanced when derivative singularities are provided for. Thus two recurring problems of integral methods are alleviated as follows.

1) Particular problem-dependent Green's functions need not be found.

2) Difficulties associated with singularity of Green's functions are side-stepped.

The advantages of the partial differential-equation approach are as follows.

1) Inhomogeneities and anisotropies are fairly easily provided for.

2) The problem is formulated as the solution of a positive-definite system.

In summary, this paper has attempted to show how

to use the partial differential and integral techniques, each in its appropriate region, to solve problems that could be intractable by either one individually.


### Acknowledgment

The authors wish to thank their colleagues for the assistance given them. They wish to thank D. J. Richards, for his excellent programming, and M. C. Décreton for many stimulating discussions about integral equations, Green's functions, and singularities.


### References


[1] F. S. Acton, *Numerical Methods That Work*. New York: Harper & Row, 1970, pp. 410–430.
[2] I. A. Cermak and P. Silvester, "Solution of two-dimensional field problems by boundary relaxation," *Proc. Inst. Elec. Eng.*, vol. 115, pp. 1341–1348, Sept. 1968.
[3] ——, "Analysis of coaxial line discontinuities by boundary relaxation," *IEEE Trans. Microwave Theory Tech. (Special Issue on Computer-Oriented Microwave Practices)*, vol. MTT-17, pp. 489–495, Aug. 1969.
[4] P. Silvester and M. S. Hsieh, "Finite-element solution of 2-dimensional exterior field problems," *Proc. Inst. Elec. Eng.*, vol. 118, no. 12, pp. 1743–1747, Dec. 1971.
[5] F. Sandy and J. Sage, "Use of finite difference approximations to partial differential equations for problems having boundaries at infinity," *IEEE Trans. Microwave Theory Tech.* (Corresp.), vol. MTT-19, pp. 484–486, May 1971.
[6] D. Greenspan and P. Werner, "A numerical method for the exterior Dirichlet problem for the reduced wave equation," *Arch. Ration. Mech. Anal.*, vol. 23, pp. 288–316, 1966.
[7] D. J. Richards and A. Wexler, "Finite-element solutions within curved boundaries," *IEEE Trans. Microwave Theory Tech.*, vol. MTT-20, pp. 650–657, Oct. 1972.
[8] A. Wexler, "Finite-element field analysis of an inhomogeneous, anisotropic, reluctance machine rotor," presented at the IEEE Summer Power Meeting, San Francisco, Calif., July 9–14, 1972, Paper T 72 422-4, to be published in *IEEE Trans. Power App. Syst.*
[9] M. C. Décreton and A. Wexler, "The care and treatment of singularities in the finite-element method," to be published.
[10] I. Stakgold, *Boundary Value Problems of Mathematical Physics*, vol. II. New York: Macmillan, 1968.
[11] H. A. Wheeler, "Transmission-line properties of parallel strips separated by dielectric sheet," *IEEE Trans. Microwave Theory Tech.*, vol. MTT-13, pp. 172–185, Mar. 1965.
[12] T. G. Bryant and J. A. Weiss, "Parameters of microstrip transmission lines and of coupled pairs of microstrip lines," *IEEE Trans. Microwave Theory Tech. (1968 Symposium Issue)*, vol. MTT-16, pp. 1021–1027, Dec. 1968.
[13] W. R. Smythe, *Static and Dynamic Electricity*. New York: McGraw-Hill, 1968, p. 115.
[14] S. G. Mikhlin, *Variational Methods in Mathematical Physics*. New York: Macmillan, 1964.
[15] R. F. Harrington, *Time Harmonic Electromagnetic Fields*. New York: McGraw-Hill, 1961.
[16] P. Silvester, "High order polynomial triangular finite-element for potential problems," *Int. J. Eng. Sci.*, vol. 7, pp. 849–861, 1969.
[17] A. Wexler, "Computation of electromagnetic fields," *IEEE Trans. Microwave Theory Tech. (Special Issue on Computer-Oriented Microwave Practices)*, vol. MTT-17, pp. 416–439, Aug. 1969.
[18] O. C. Zienkiewicz, *The Finite Element Method in Engineering Science*. London, England: McGraw-Hill, 1971.


# Short Papers

## A Method for Computing Edge Capacitance of Finite and Semi-Infinite Microstrip Lines

T. ITOH, R. MITTRA, AND R. D. WARD

***Abstract*—This short paper describes a method for computing the edge capacitance of finite or semi-infinite sections of microstrip transmission lines. The approach is based on Galerkin's method applied in the Fourier-transform domain. It is mathematically simple and requires the inversion of rather small-size matrices.**

### Introduction

In this short paper, a new method is developed for calculating the fringe (excess) capacitance due to an abrupt truncation of a uniform microstrip line. In contrast to the conventional matrix formulation in the space domain, the method to be presented here is based upon an application of Galerkin's method in the spectral or Fourier-transform domain. The spectral-domain approach has been successfully applied to a number of other problems [1]–[3]. It is particularly suitable for handling open-region problems of the type considered in this short paper.

Manuscript received March 27, 1972; revised July 3, 1972. This work was supported in part by the United States Army Research Office under Grant DA-ARO-D-31-124-71-G77 and in part by the National Science Foundation under Grant GK 15288. The major portion of this paper was presented at the 1972 IEEE G-MTT International Symposium, Chicago, Ill., May 22–24, 1972.

T. Itoh and R. Mittra are with the Department of Electrical Engineering, University of Illinois, Urbana, Ill. 61801.
R. D. Ward was with the Department of Electrical Engineering, University of Illinois, Urbana, Ill. 61801. He is now with the Hughes Aircraft Company, El Segundo, Calif.

### Formulation and Method of Solution

In the TEM approximation, it is assumed that the discontinuity capacitance may be computed from the knowledge of the field solution derived in the static limit. This is done by first solving Poisson's equation for the potential function $\phi$ for the geometry under consideration. (The geometry is shown in Fig. 1.) This, in turn, requires the solution of the equation

$$\nabla^2\phi(x, y, z) = -\frac{1}{\epsilon_o}\rho(x, z)\delta(y)$$
$$\rho(x, z) = 0, \quad |x| > W/2, \quad |z| > l/2 \tag{1}$$

where $\epsilon_o$ is the free-space permittivity, $\delta(y)$ is the delta function, and $\rho(x, z)$ is the charge distribution on the strip. The strip is assumed to have infinitesimal thickness and to be perfectly conducting. The ground plane and the dielectric substrate are also assumed to be lossless. Next, we introduce the two-dimensional Fourier transform of the potential $\phi$ via

$$\tilde{\phi}(\alpha, y, \beta) = \int_{-\infty}^{\infty}\int_{-\infty}^{\infty}\phi(x, y, z)\exp j(\alpha x + \beta z)\,dxdz. \tag{2}$$

Taking the transform of (1), we obtain

$$\left[\frac{\partial^2}{\partial y^2} - (\alpha^2 + \beta^2)\right]\tilde{\phi}(\alpha, y, \beta) = -\frac{1}{\epsilon_o}\tilde{\rho}(\alpha, \beta)\delta(y) \tag{3}$$

where $\tilde{\rho}$ is the transform of charge distribution defined by

$$\tilde{\rho}(\alpha, \beta) = \int_{-l/2}^{l/2}\int_{-W/2}^{W/2}\rho(x, z)\exp j(\alpha x + \beta z)\,dxdz. \tag{4}$$